Crystallisation in flow Part I: paleo-circulation track by texture analysis and magnetic fabrics.

Stanislas Sizaret, Yan Chen, Luc Barbanson, Bernard Henry, Pierre Camps, Eric Marcoux

Crystallisation in flow Part I: paleo-circulation track by texture analysis and magnetic fabrics

Stanislas Sizaret [a,b,*], Yan Chen [b], Luc Barbanson [b], Bernard Henry [c], Pierre Camps [d], Eric Marcoux [b].

[a] Physico-chemical Geology, K.U. Leuven, Celestijnenlaan 200C, B-3001 Heverlee, Belgium.

[b] ISTO, Université d'Orléans, 45067 Orléans cedex 02, France.

[c] IPGP, 4 avenue de Neptune, 94107 Saint-Maur cedex, France

[d] CNRS and Université Montpellier 2 34095 Montpellier cedex 5, France

[*] Corresponding author:

E-mail address: Stanislas.Sizaret@univ-orleans.fr

SUMMARY

In order to better define the dependence of the mineral texture on flow, Anisotropy of Magnetic Susceptibility (AMS) and microscopic observations have been performed on calcite rich precipitations occurring in a horizontal pipe where the flow direction is clearly defined. Sixty-five cubes were cut from 5 slices, magnetic studies identified-pseudo-single domain magnetite as the major AMS carrier. Horizontal foliation characterizes the magnetic fabrics and the lineation is parallel to the pipe axis, i.e. the flow direction. The origin of this lineation is discussed and is interpreted to be mainly the consequence of elongated pseudo single domain magnetite. To complete the magnetic fabric studies, shape preferred orientation statistics were performed on 563 calcite sections in the (0001) calcite plane. It shows elongated shapes with a general orientation parallel to the pipe axis. The mean shape orientation is the average of two distinct sub-populations that deviated slightly from the pipe

axis. Observation on calcite shapes and the direction of the magnetic lineation are coherent, suggesting that it is possible to track hydrothermal paleo-circulation using magnetic lineation and petrographic fabrics.

Key words: Fluid dynamics, Rock magnetism, Magnetic susceptibility, Crystallography.

1 INTRODUCTION

Paleocirculation in mineralised veins is generally reconstructed on a kilometer scale by theoretical calculation and simulation using finite element method (e.g. Barnes 1997; Roure et al. 2005). No method providing direct information from observation in-situ has been proposed until now to reconstruct these complex flows. Though the effect of fluid flow is largely evoked in the literature, it is rarely used to interpret these observations in term of fluid circulation (e.g. Lebedev 1967; Kessler *et al.* 1972; Garside *et al.* 1975; Prieto & Amoros 1981; Kostov & Kostov 1999; Hilgers & Urai 2002; Chernov 2004). The recent textural study on Jurassic hydrothermal veins and their surrounding sandstone, combining microscopic observations and AMS measurements shows a good correlation between magnetic lineation, mineral textures and fluid flow direction deduced from sedimentary and tectonic structures (Sizaret *et al.* 2003). This work presents a potential method to reconstruct the paleocirculation by magnetic fabrics and mineralogical study. Nevertheless, the link among textures, magnetic fabrics and hydrodynamics remains to be confirmed by theoretical modelling and natural case studies on mineral deposits where the flow direction is clearly constrained. This is why we carried out two successive studies on calcite-rich deposits from a hydrothermal spring in Chaudes-Aigues (French Massif Central). Part I presents an analytical study of mineral fabrics and Part II concerns a theoretical interpretation of these data.

The aim of this study is to establish a relationship among directional flow, mineral texture and magnetic fabrics. This work concerns a simple and well-defined geological situation: a calcite-rich precipitate formed in a horizontal pipe channelling hot water from the hydrothermal spring in Chaudes-Aigues (French Massif Central). To analyse the mineralogical textures and magnetic fabrics, two methods have been applied: microscopic observations with cathodoluminecence and AMS measurements. Optical observation shows that the differential growth rate on crystal faces is related to the different exposure of these faces with respect to the flow. Magnetic fabrics are usually interpreted in terms of grain orientation by mechanical rotation in a highly viscous media or recrystallisation in a stress field (Tarling & Hrouda 1993). However, in this paper, we will show that the magnetic fabrics depend on the anisotropic crystal growth in the context of hydrothermal flow.

2 GEOLOGICAL SETTING

The calcite precipitates are formed by a hot spring located at Chaudes-Aigues in the French Massif Central. This hydrothermal activity is related to a mantle upwelling, which produced an important alkaline volcanic activity during the Neogene (e.g. Vasseur *et al.* 1997).

Located in the southern part of the volcanic region, Chaudes-Aigues springs produce the hottest water of Europe (82°C). It has a mineral concentration close to 940.5 mg/l with pH=6.3. According to isotopes, chemical data and hydrodynamic calculation, Vasseur *et al.* (1997) and Négrel *et al.* (2000) propose a genetic model involving a superficial circulation of low salinity water and a deep circulation of mineralised fluids. At Chaudes-Aigues, the hot water is conducted by polyvinyl chloride pipes for the purposes of heating houses and medical therapy treatments. This installation operates about 7 months a year, and the studied pipe was filled by calcite between 1994 and 1998 (Fig. 1a). Chemical analysis of the source du Ban (40

l/min; 70°C) shows P_{CO2}=O.6 bars and the product of activity of CO_3^{2-} (= 1.55 10^{-6}) with Ca^{2+} (= 9.09 10^{-4}) is less than the solubility product of calcite ($pK_S^{70°C}$ = 8.86) (Vasseur *et al.* 1997). At the entrance of the pipe, the water is undersaturated with respect to calcite, the rapid degassing of CO_2 increases the pH and precipitates the calcite.

The pipe has been sampled in horizontal position. To simplify the geometric projection, the pipe axis is oriented with the N-S direction. In order to characterize the texture, three perpendicular thin sections were made with respect to the calcite bands (Fig. 1a): (i) vertical and along the pipe axis, i.e. perpendicular to calcite bands, (ii) vertical and parallel to the pipe section and (iii) horizontal, i.e. parallel to the calcite bands. Sixty-five cubes of 2x2x2cm^3 were cut from 5 slices of the pipe for the magnetic fabric study.

3 MINERALOGICAL STUDY

The mineralogical composition of precipitated materials was determined using microprobe observations, X-ray diffraction (Diffractometer I.N.E.L, with Co anticathode and curved detector 0-120°), Scanning Electronic Microscopy (SEM, Jeol 6400 appartus) and thermomagnetic curve performed with an oven of AGICO CS3 coupled with a Kappabridge. To investigate the magnetic mineralogy, magnetic hysteresis loops were determined with a magnetic field of up to 1.0 Tesla (magnetic inductrometer at IPGP).

Figure 1

X-ray diffraction and microscopic observations show that the mineral composition is largely dominated by calcite (Figs 1b, 1c and 1d) . On the calcite faces and within the crystals, inclusions of thin dendrites of iron oxides occur, giving the dark bands observed in calcites (Figs 1b, 1c and 1f).

Figure 2

Thermomagnetic curves were acquired by monitoring changes in magnetic susceptibility between room temperature and 700 °C in inertial Argon gas. The magnetic susceptibility increases up to 350°C, (Fig. 2). Partial cooling curve performed at 325°C is different from the heating curve suggesting mineralogical transformation at low temperature. After 500°C, the susceptibility increases drastically. This could be coeval to transformation of iron rich calcite in hematite or magnetite (Dunlop & Özdemir 2000; Dekkers 1990). Partial reverse curve at 525°C shows an important mineralogical transformation forming new mineral with higher magnetic susceptibility. The next decreases of susceptibility due to heating is observed between 500° and 600°C suggesting the presence of magnetite, no significant drop has been observed at the hematite Curie temperature (680°C; Fig. 2; Borradaile & Henry 1997). During cooling the susceptibility drastically increases below 585°C, suggesting that magnetite has been formed at high temperature with iron reduction.

Figure 3

The study of the magnetic mineralogy is completed by magnetic hysteresis loop performed on 12 samples of about 1 cm^3 . Specimens are submitted to a variable magnetic field. The magnetic lag between the external field and induced magnetic moment determines a hysteresis loop, which characterizes magnetic properties of samples (e.g., Day *et al.* 1977; Dunlop & Özdemir 1997). Table 1 presents the results obtained on the samples taken from a pipe cross section. Figures 3(a) and 3(b) present the dominant effect of the paramagnetic minerals at higher magnetic field and a secondary effect due to ferromagnetic minerals at low field, respectively. The paramagnetic minerals are probably carried by Fe-rich calcite

(Rochette *et al.* 1992). After removing the paramagnetic component (Fig. 3b), the ferromagnetic signal is characterized by a magnetization average ratio of Mrs/Ms = 0.17 and a coercivity ratio of Hcr/Hc=2.5 (Table 1), suggesting the presence of pseudo single domain magnetite (Fig. 3c; e.g. Day *et al.* 1977; Dunlop & Özdemir 1997).

4 MINERAL TEXTURES AND MAGNETIC FABRICS

The whole precipitate is composed of eighteen bands of thickness varying from 1 to 3 mm (Fig. 1a). The older bands do not cover all the wall of the pipe section (Fig. 1a) because, at the beginning of the pipe installation, the hydrothermal fluid did not fill the pipe. The successive bands mark the fluid level in the pipe and show the progressive reductions of the flow section. The texture evolved gradually from older to younger layers. The oldest layers are relatively compact and the crystals boundaries are in contact (Figs 1b, 1c and 1e); the younger layers are relatively isolated rising within the flowing solution (Fig. 1d). Calcite presents syntaxial growth, some vacuoles are observed at the bottom of the bands and in the upper part, calcite crystallizes in radiating sheaf structures (Figs 1b and 1c). Goniometric measurements have been performed with an I.N.E.L apparatus XRG 3000; CPS 120, with a Co anticathode and a curve detector 0-120°. The variation of the diffraction intensity is measured for all the spatial orientation of the sample. The result gives an image of the lattice preferred orientation (LPO) in the sample. It confirms the high angle varying from 60° to 90° between the calcite <c> axes and the precipitation surface (Fig. 4a).

Optical investigations were performed on the three specific oriented sections as shown on Figure 1(a) and following phenomenon are observed.

i) In vertical section parallel to the pipe axis, horizontal dark bands suggest a specific distribution of iron oxides (Fig. 1b). Growth bands could be observed by

cathodoluminescence and suggest that the main growth direction is vertical along the <c> axis (Fig. 1d);

ii) In the plane of the pipe section, dark bands are horizontal. They underline the mammillary precipitation surfaces and are perpendicular to the average direction of the calcite <c> axis (Fig. 1d);

iii) In the horizontal plane, calcite shows elongated habits (Fig. 1e, 4b). It occurs mostly as batches with thinner faces developed in upstream position and larger faces with dark bands in downstream position; crystal edges are mostly concaves. In this plane the growth band observed in cathodoluminescense has variable thickness (Fig. 4b). Upstream faces have thicker growth bands, the highest growth rate occurs on the faces that have a relatively low angle with the flow direction. The inertia moment method is used to model crystal sections by ellipses and to estimate their axis length and trend (Launeau & Robin 1996; Grégoire *et al.* 1998). Statistics on 561 measurements were used to characterise these sections by an ellipse with its average elongation orientation parallel to the pipe and a mean ellipticity ratio of 2. This bulk average trending is the result of two sub-populations with mean directions of 347°±5° and 16°±5° with respect to the N-S orientated pipe (Fig. 4c). The plane (0001) perpendicular to <c> axis is supposed to have isotropic crystallographic properties. The thin section suggests that this (0001) plane has an elongated shape. However it should be noticed that is not the consequence of the calcite <c> axis projection in the thin section plane. If the elongated shape with an ellipticity of 2 was due to projection, it would suppose an average angle of 60° between <c> axis and the section of the isotropic plane (ellipticity of 1), which is in contradiction with the goniometric measurements performed on calcite (Fig. 4a). Therefore, the observed mineral lineation in thin

sections of Figure 1e is not an artefact but the consequence of the calcite elongated (0001) plane perpendicular to <c> axis.

Figure 4

To study the magnetic fabrics, AMS measurements were performed at low magnetic fields with a AGICO KLY-3S kappabridge at Institut des Sciences de la Terre d'Orléans. The spatial variation of the susceptibility could be described by an ellipsoid with three principal axes of magnetic susceptibility. The long axis ($\mathbf{K_{max}}$) defines the magnetic lineation; the short axis ($\mathbf{K_{min}}$) corresponds to the pole of the magnetic foliation defined by the ellipsoid plan containing $\mathbf{K_{max}}$ and $\mathbf{K_{int}}$ (intermediate axis). The degree of anisotropy and the shape can be quantified by [1]*P'* and [2]*T*, respectively (Jelinek 1981); When *P'*=1, the magnetic fabrics is isotropic. *P'* increases with the degree of anisotropy, positive or negative *T* value discriminates magnetic fabrics that are dominated by the foliation (oblate) or lineation (prolate), respectively. The shape and the orientation of the ellipsoid depend on three parameters: the preferred orientation of magnetic crystal lattice, the shape of the susceptibility carrier and the distribution of grains in the sample (Tarling & Hrouda 1993; Hrouda 1982).

Table 1

The pipe section is divided in 13 sites and five samples from each site are measured. The average direction and magnetic fabric parameters are calculated independently from each other for each site (i.e. the calculation is simple arithmetic mean and not an average of tensor). The magnetic fabrics has a relatively low degree of anisotropy ($P'_{average}$=1.054) with a

[1] $P'=\exp\{2[(\ln K_{max}-\ln K_m)^2+(\ln K_{int}-\ln K_m)^2+(\ln K_{min}-\ln K_m)^2]\}$, $K_m=(\ln K_{max}+\ln K_{int}+\ln K_{inf})/3$

[2] $T=[2\ln(K_{int}/K_{min})/\ln(K_{max}/K_{min})]$, T>0 oblate, T<0 prolate

[2]

dominant oblate shape ($T_{average}$=0.585; Table 2). The *P'* values for individual sites have a low standard deviation except for the site 12 where the anisotropy is higher (Table 2 and Fig. 5a). The mean value of *P'* in the pipe increases from bottom to the top with a gradient parallel to the calcite band. This behaviour is not an artefact due to high value of the site 12 as the neighbours sites 11 and 13 are relatively high (Fig. 5a). The shape value *T* presents relatively high standard deviation and the distribution of the value is approximately organised with a centripetal increase (Fig. 5b); this variation is not linked to P' nor to the $\mathbf{K_{max}}$ orientation (Fig 6).

Figure 5

Figure 6

The orientation of the principal axes is constant, whereby the foliation pole ($\mathbf{K_{min}}$) is subnormal to band in the pipe. In the western sites, $\mathbf{K_{min}}$ dip towards E (Figs 7a-d and 7k), in the eastern sites towards W (Figs 7g-j and 7m) and in the middle the $\mathbf{K_{min}}$ dip is vertical (Figs 7e-f and l). The dip variation reflects the symmetry of the calcite band orientation (Fig. 7n). The magnetic foliation largely dominates the fabrics, however the lineation is also clearly present and parallel to the pipe orientation except for the sites d and f. The shape of the 95% interval of confidence calculated with the bivariate statistics shows possible exchange between $\mathbf{K_{max}}$ and $\mathbf{K_{int}}$ due to the dominance of the oblate shape (Le Goff 1990; Le Goff *et al.* 1992). Plotting the measurement on the 65 sites increase the accuracy of $\mathbf{K_{max}}$ orientation and the bivariate statistics show a slight deviation of $\mathbf{K_{max}}$ from the pipe axis (Fig. 7o). This deviation may be due to the distribution of $\mathbf{K_{max}}$ orientations near E-W.

Figure 7

At low magnetic field, weakly coercive magnetic minerals, i.e. magnetite in our case, dominate the magnetic susceptibility (Tarling & Hrouda 1993; Rochette *et al.* 1992). Magnetic fabrics is therefore controlled by dendritic magnetite (crystal with arborescent structure, Fig. 1f). However, when the bulk magnetic susceptibility is very low with high *P'* values the AMS could result from a relatively important contribution of the diamagnetic phases (Hrouda, 1986). To determinate the mineral carrier of the anisotropy of magnetic susceptibility, Anhysteretic Remanent magnetization (ARM) experiment has been performed on 2 samples and these results are compared to those of AMS (McCabe et al. 1985).

The ARM measurements were carried out by three step using a 2G cryogenic SQUID magnetometer with an AF demagnetizer at the University of Montpellier 2 (France). The sample was first demagnetized with an alternating field (AF) along 3 perpendicular axes with a maximum magnetic field of 140 mT. In a second time, an ARM is acquired along a direction perpendicular to the last demagnetized axis with a bias direct field of 100 μT and AF of 120 mT. In the third step the induce ARM was measured. These three steps are repeated for 9 positions. The remanent anisotropy is modelled by ellipsoid constructed from the axial measurements plus the off-axis remanence terms. This represents 27 measurements. The results of this experiment depend on susceptibility values. Samples with susceptibility higher than 70 $x10^{-6}$ SI show a good agreement of ARM axes (maximum intermediate and minimum) with respect to corresponding AMS ones (see Figs 8a). This confirms that the AMS reflects the magnetic fabric of magnetic grains. For samples with lower magnetic susceptibility, the case is more complex. Because of various grain sizes of magnetite with coexistence of single domain and pseudo single domain, a gyromagnetic remanent magnetization (GRM) seems to be produced during the AF treatment and then influences the ARM analysis (Stephenson 1981, Dunlop & Özdemir 1997). After this artefact has been removed by considering only the magnetic remanent component acquired in the direction of

the applied field, the results of ARM for the samples with weak susceptibility show also consistent orientations with respect to AMS ones (Fig. 8b). A detailed analyses to identify a GRM and to minimize its effect will be discussed in another paper since it is out of the scope of this investigation.

Figure 8

5 DISCUSSIONS AND CONCLUSIONS

Calcite displays a radiating fibrous structure in vertical sections, the <c>-axis trend is perpendicular to the precipitation surface, as shown by the optic observations and goniometric (LPO) measurements (Figs. 1b, 1c and 1d). This crystal texture is quite common for calcite in the hydrothermal context. The formation of such texture is usually explained by competitive growth with a selective elimination of those crystals in which the <c> axes are not perpendicular to the substrate (Gonzàles *et al.* 1992). In the horizontal (0001) plane, i.e. that perpendicular to the <c> axis, crystal sections sometimes present triangular shapes, but elongated forms are dominant as demonstrated by shape analyses and goniometric studies (Figs. 4a and 4c). As elongated shapes do not correspond to the trigonal symmetry of the (0001) sections, the differential growth rate observed in cathodolumiscence should be related to external forces (Curie 1908). Therefore, the lineation observed in the (0001) section should be a direct consequence of the flow. Part II of this work that follows this paper establishes the theoretical link between fluid flow and relative growth rates of crystal faces by modelling chemical diffusion through the boundary layer.

Magnetite is the main carrier susceptibility carrier of the magnetic fabric for the hydrothermal precipitate. It has very low magnetocrystalline anisotropy, therefore the magnetostrictive anisotropy will dominate when the magnetite is not euhedral (Dunlop & Özedemir, 1997). For this reason the preferential orientation of grain shapes will affect the

magnetic anisotropy (e.g., Borradaile & Henry 1997). Moreover, hysteresis analysis shows that magnetite grains are of pseudo single domain type with normal fabrics by the longer shape dimension corresponds to the maximum of the magnetic susceptibility and this behaviour is called normal fabrics (Potter & Stephenson 1988; Tarling & Hrouda 1993; Borradaile & Henry 1997).

The magnetic fabrics are dominated by oblate shape with a foliation parallel to calcite banding. Nevertheless, magnetic lineation has been clearly defined with an orientation parallel to the pipe axis. This could be interpreted as elongated magnetite grain or an intersection lineation due to folded magnetite bands. Direct observation of the magnetite grain shape is complex due to the dendritic precipitation. The presence of undulated / folded structure is clearly observed in the sites 1 and 9 (Fig. 7n). In these sites the low *T* values confirm the less intense foliation (Table 2). In other samples, the foliation is more remarkable, and the calcite banding shows relatively constant angle. Dispersion on the orientation of the lineation direction suggests that it is also sensitive to EW undulation of the calcite banding controlled by vacuoles and mammillary textures (Fig. 1b). Such textures combined with highly oblate magnetic fabrics could make easier exchanges between $\mathbf{K_{max}}$ and $\mathbf{K_{int}}$. In the flat samples with high T, N-S lineation depends on the elongated magnetite shape similarly to the calcite microscopic observation. No significant correlation has been observed between the $\mathbf{K_{max}}$ orientation and the shape value *T* (Fig. 7o). The variation of the lineation direction from E-W to N-S is reduced by increasing the number of measurements, this variation could be explain in term of representative size of the sample to characterize the magnetic fabrics (Fig. 7n). The general lineation direction is clearly parallel to the pipe i.e. to the fluid flow.

The magnetite is assumed to have crystallised from the hydrothermal solution because the dendritic shape and precipitation conditions in a closed environment allow the majority of magnetite to nucleate and growth on the pipe wall without transport or settlement as detrital

grains. The magnetic lineation parallel to the pipe axis, i.e. to the flow direction, could be explained by elongated shapes by analogy with the calcite. The fluid flow should control the crystal shape through the crystal growth process. This interpretation justify the use of the magnetic lineation as marker of the hydrothermal flow direction as suggested in previous study even in case of complex mineral textures (Sizaret *et al.* 2003).

Crystal growth should be controlled by fluid flow as suggested by the magnetic lineation and the anisotropy of magnetite crystal growth could be compared to the calcite.

This study is a further example that mineral lineations measured by both magnetic and optical methods are parallel to the flow direction in hydrothermal formations. AMS coupled with mineral texture analysis may be considered as a powerful method to reconstruct hydrothermal flow path in ancient formations. The AMS method shows a good efficiency and allows to make subsequent statistical observation. However, such paleo-circulation reconstruction should be justified by the interpretation on the lineation origin that should link to crystal growth process in flowing solution discussed in Part II of this study.

Acknowledge.

This study was supported by the Région Centre Scholarship for the first author. We present our thanks to Fatima Martin-Hernandez and anonymous reviewer for their constructive critics to improve the manuscript.

REFERENCES

Barnes H-L., 1997. *Geochemistry of hydrothermal ore deposits*, 3rd edn, pp. 125-191, John Wiley & Sons, New York. Barnes.

Borradaile, G.J. & Henry, B., 1997. Tectonic applications of magnetic susceptibility and its anisotropy, *Earth Sci. Rev*., 42, 49-93.

Chernov, A.A., 2004. Notes on interface growth kinetics 50 years after Burton, Cabrera and Frank, *J. of Crystal Growth*, 264, 499-518.

Curie, P., 1908. *Œuvres*, , 118p Gautier-Villars, Paris, Société Française de Physique. Reprinted : Archives contemporaines, Paris 1984.

Day, R., Fuller, M.D., & Schmidt, V., 1977, Hysteresis properties of titanomagnetites: Grain size and composition dependence, *Phys. Earth Planet. Int.*, 13, 260-267

Dunlop, D.J. & Özdemir, Ö., 1997. *Rock Magnetism fundamentals and frontiers*, pp. 74-76, Univ. Press, Cambridge.

Garside, J., Janssen-van Rosmalen, R. & Bennema, P., 1975. Verification of crystal growth rate equations, *J. of Crystal Growth*, 29, 353-366.

Gonzàles, L.A, Carpenter S.J. & Lohmann K.C., 1992. Inorganic calcite morphology: Roles of fluid chemistry and fluid flow, *J. Sediment. Petrol*., 62, 382-399.

Granet, M., Wilson, M. & Achauer, U., 1995. Imaging a mantle plume beneath the French Massif central, *Earth Planet. Sci. Lett.*, 136, 281-296.

Grégoire, V., Darroze, J., Gaillot, P., Nedelec, A. & Launeau, P., 1998. Magnetite grain shape and distribution anisotropy vs. rock magnetic fabric: a three-dimensional case study, *J. Str. Geol.*, 20, 937-944.

Henry, B. & Le Goff,M., 1995. Application de l'extension bivariate de la statistique de Fisher aux données d'anisotropie de susceptibilité magnétique: integration des incertitudes de measures sur l'orientation des directions principales. *C. Acad. Sc. Paris*, 320, II, 1037-1042.

Hilgers, C. & Urai, J.L., 2002. Experimental study of syntaxial vein growth during lateral fluid flow in transmitted light: first results, *J. Str. Geol.*, 24, 1029-1043.

Hrouda, F., 1982. Magnetic anisotropy of rocks and its application in geology and geophysics, *Geophys. Surv.*, 5, 37-82.

Hrouda, F., 1986. The effect of quartz on the magnetic anisotropy of quartzite, *Studai geoph. et geod.*, 30, 39-45.

Jelinek, V., 1981. Characterization of the magnetic fabric of the rocks, *Tectonophysics*, 79, 63-67.

Kessler, S.E., Stoiber, R.E. & Billings, G.K., 1972.Direction of flow mineralizing solutions at Pine Point, N. W. T., *Econ. Geol.*, 67, 19-24.

Kostov, I. & Kostov, R.I., 1999. *Crystal Habits of Minerals*, 415 pp. Pensilvania, Sofia,.

Launeau, P. & Robin, P-Y-F., 1996.Fabric analysis using the intercept method, *Tectonophysiscs* 267, 91-119.

Le Goff, M., 1990. Lissage et limites d'incertitudes des courbes de migration polaire : pondération, des données et extension bivariate de la statistique Fischer, *C. R. Acad. Sci. Paris*, 311 II, 431-437.

Le Goff, M., Henry, B. & Daly, L., 1992. Practical method for drawing a VGP path, *Phys. Earth Planet. Inter.*, 70, 201-204

Lebedev, L.M., 1967. Metacolloid in Endogenic Deposits, 298 pp. Plenum Press, New York.

McCabe, C., M., Jackson & Ellwood, B.B., 1985. Magnetic anisotropy of the Trenton limestone results of a new technique, anisotropy of anhysteretic susceptibility, *Geophys. Res. Lett.*, 12, 333-336.

Négrel, P., Guerrot, C., Cocherie, A., Azaroual, M., Brach, M. & Fouillac, C., 2000. Rare earth elements, neodymium and strontium isotopic systematics mineral waters: evidence from the Massif Central, France, *Appl. Geochem.*, 15, 1345-1367.

Prieto, M. & Amoros, J.L., 1981. On the influence of hydrodynamic environment on crystal growth, *Bull. Minéral.*, 104, 114-119.

Potter, D.K., & Stephenson A., 1988. Field-impressed magnetic anysotropy in rocks, Geophys. Res. Lett., 15, 1097-1100.

Rochette, P., Jackson, M. & Aubourg, C., 1992. Rock magnetism and the interpretation of anisotropy of magnetic susceptibility, *Geophys. Rev.*, 30.3, 209-226.

Roure, R., Swennen, R., Schneider, F., Faure, J.L., Ferket, H., Guilhaumou, N., Osadetz, K., Robion, P., & Vandeginste, V., 2005. Incidence and importance of tectonics and Natural fluid migration on reservoir evolution in Foreland Fold and thrust belts, *Oil & Gas Science and Technology – Rev. IFP, 60, 67-106*

Sizaret, S., Chen, Y., Chauvet, A., Marcoux, E. & Touray, J.C., 2003. AMS fabrics and fluid flow directions in hydrothermal systems, A case study in the Chaillac Ba-F-Fe deposits, *Earth Planet. Sci. Lett.*, 206, 555-570.

Stephenson A., 1981. Gyromagnetic remanence and anisotropy in single –domain particles, rocks and recording tape, *Phil. Mag.*, B44, 635-664.

Tarling, D.H. & Hrouda F., 1993. *The magnetic anisotropy of rocks*, pp. 217, Chapman & Hall, London.

Vasseur, G., Michard, G. & Fouillac C., 1997. Contraintes sur la structure profonde et le fonctionnement du système hydrothermal de Chaudes-Aigues (France), *Hydrogéologie*, 4, 3-17.

FIGURE AND TABLE CAPTIONS

Figure 1. Precipitates in the Chaudes-Aigues horizontal pipe. (a) Pipe section showing calcite bands; (b) Radiating sheaf texture vertical and parallel to the pipe axis. Vac = vacuole; (c) Sheaf textures observed in the vertical section of the pipe; (d) Crystal of the last calcite band rising in the flowing solution (Cathodoluminescense); (e) Calcite textures in the plane horizontal with elongated shapes; (f) Electron back-scattering image of a vertical section (SEM) showing aragonite (Arg) and dendrites of magnetite (Mgt);

Figure 2. Magnetic susceptibility variation versus temperature.

Figure 3. Hysteresis loops before (a) and after (b) removing paramagnetic mineral contribution to induced magnetic moment; (c) Day et al. (1977) plot M_{rs}/M_s versus H_{cr}/H_c

Figure 4. Analysis of the calcite texture. (a) Lattice preferred orientation of the (0001) pole plane i.e. the calcite <c> axis, the grey levels indicate the diffracted X-ray intensities; (b) Growth bands in calcite section cut in the horizontal plane (Cathodoluminescense); (c) Distribution of the calcite long axes in the plane normal to the <c> axis. These statistics have been performed on a thin section of 3.5 x 2.5 mm^2.

Figure 5. Maps of the AMS parameter variation in the pipe section. (a) the degree of anisotropy *P'* and (b) the shape parameter *T*.

Figure 6. Shape parameter *T* versus $\mathbf{K_{max}}$ deviation diagram.

Figure 7. Pipe section showing the different sites analysed and all AMS results projected in equal-area lower hemisphere. (a)-(m) on each sites five samples are measured, their average trend with the 95% interval of confidence is presented. (m) represents the pipe section with the different site area; (o) grey symbols stand for AMS results from each specimen and black ones for averages with their 95% confidence intervals.

Figure 8. Stereograph comparing the principal axis of AMS (grey) and ARM (black) the circle gives the interval of confidence at 95 %, the study has been performed on: (a) sample with a susceptibility relatively high (80 SI) coming from the site 1, (b) sample with lower susceptibility (20 SI) from the site 2.

Table 1. Saturation remanent magnetization, saturation magnetization ratio (M_{rs}/M_s) and coercive force, coercivity of remanence ratio (H_c/H_{cr}). M_{rs}, M_s and H_c are deduced from hysteresis loop after correction of the paramagnetic contribution, Hcr was determined by applying a progressively increasing backfield after saturation.

Table 2. AMS parameters characteristic of the magnetic fabric. Kv, volumetric susceptibility; s standard deviation, *P'* corrected degree of anisotropy (see text); *T* shape parameter (see text); $\mathbf{K_{max}}$, $\mathbf{K_{int}}$, $\mathbf{K_{min}}$, Directions of the maximum, intermediate and minimum ellipsoid axes, respectively. D and I, declination and inclination.

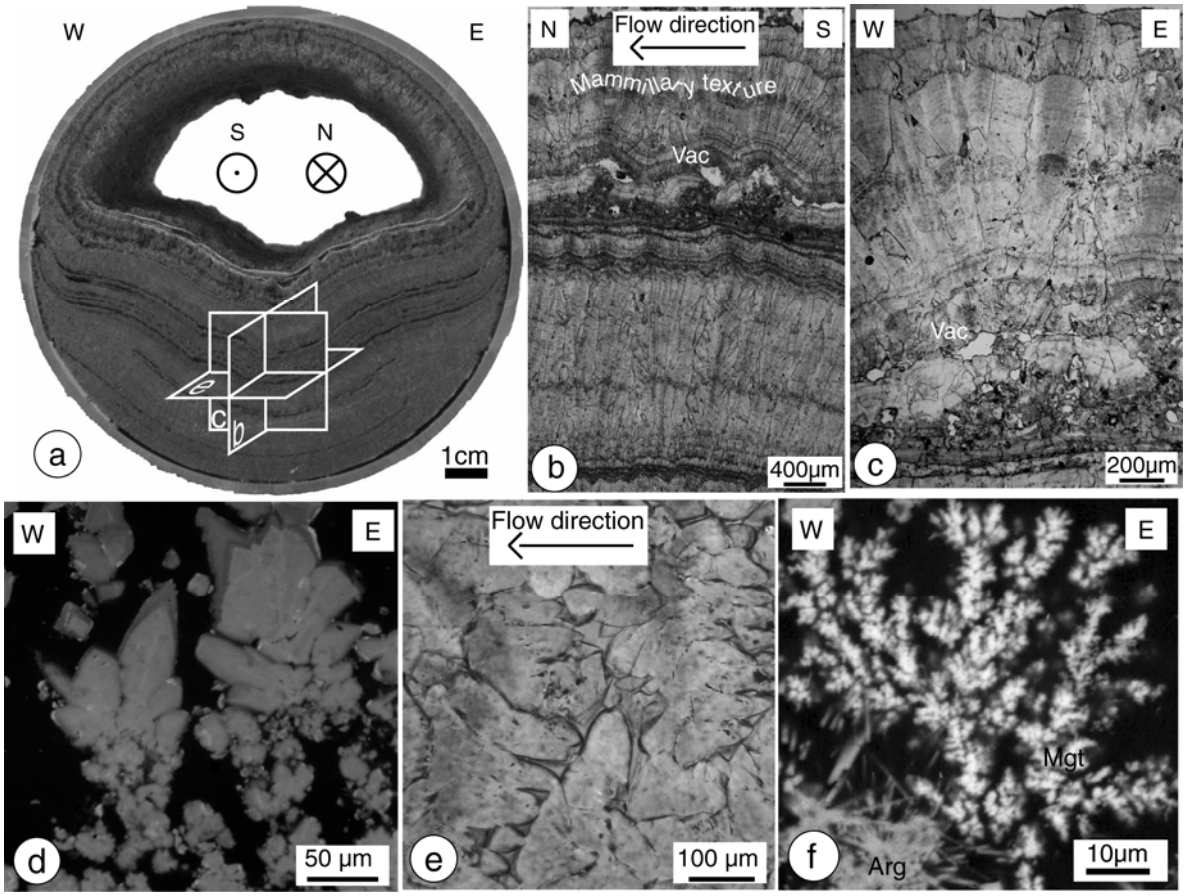
W
E
S
N
a
c
b
1cm
N
Flow direction
S
Mammillary texture
Vac
b
400μm
W
E
Vac
c
200μm
W
E
d
50 μm
Flow direction
e
100 μm
W
E
Mgt
f
Arg
10μm

FIGURE 1

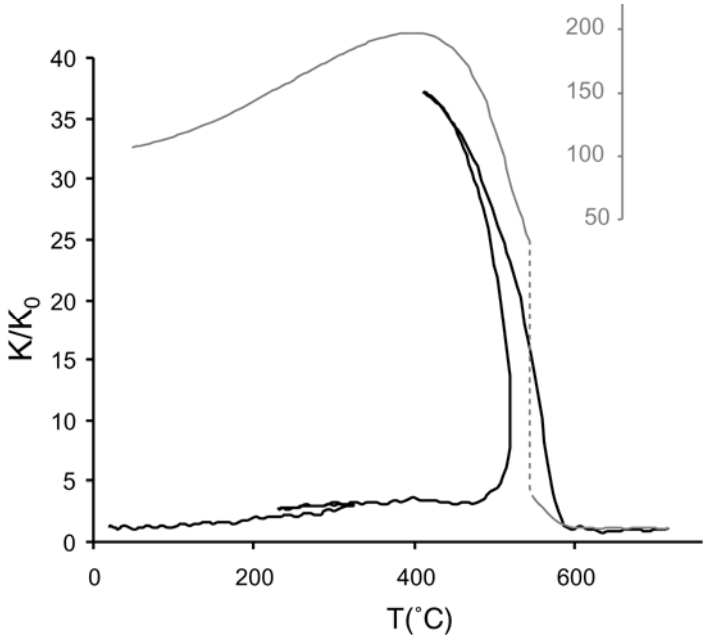

FIGURE 2

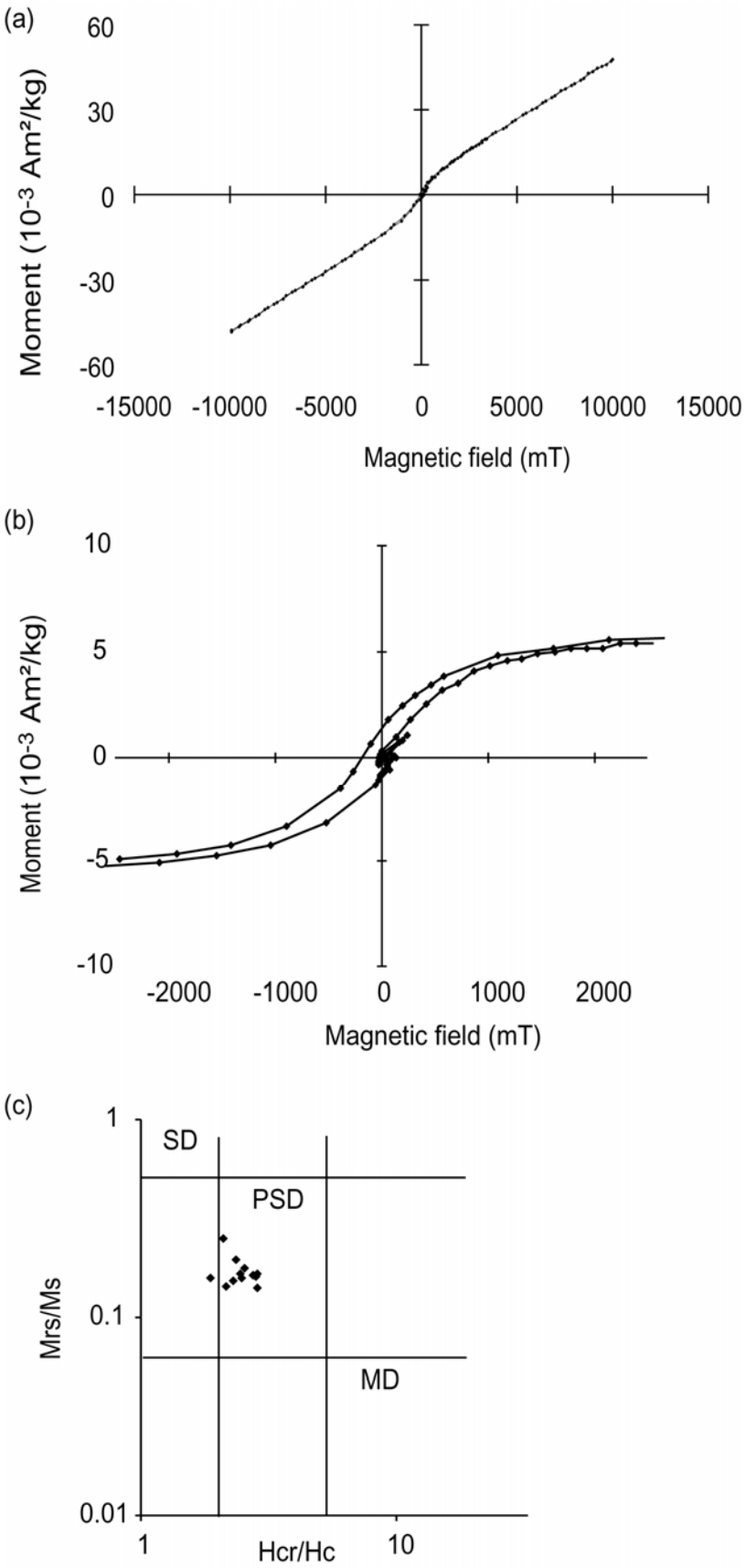
(a)
60
30
0
-30
-60
Moment (10-3 Am²/kg)
-15000
-10000
-5000
0
5000
10000
15000
Magnetic field (mT)
(b)
10
5
0
-5
-10
Moment (10-3 Am²/kg)
-2000
-1000
0
1000
2000
Magnetic field (mT)
(c)
1
SD
PSD
0.1
MD
0.01
Mrs/Ms
1
Hcr/Hc
10

FIGURE 3

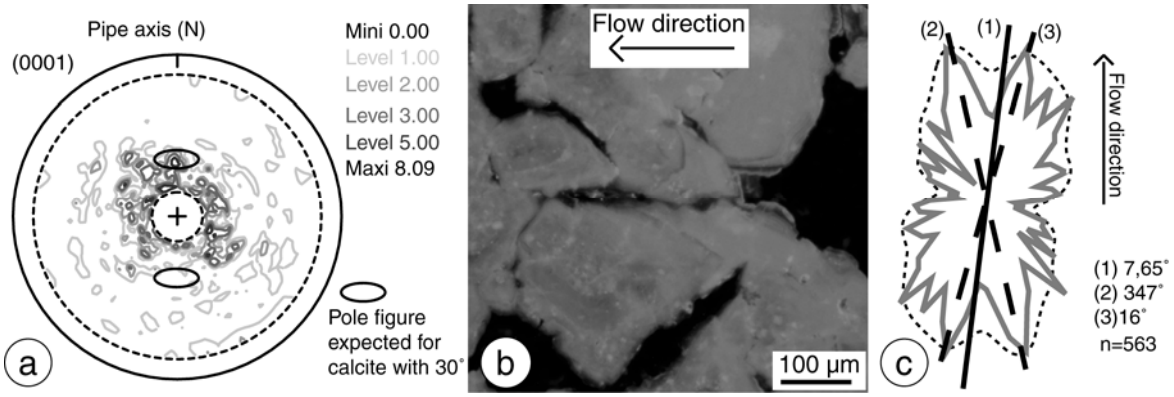
Pipe axis (N)
(0001)
Mini 0.00
Level 1.00
Level 2.00
Level 3.00
Level 5.00
Maxi 8.09
Pole figure
expected for
calcite with 30°
a
Flow direction
b
100 µm
(2)
(1)
(3)
Flow direction
c
(1) 7,65°
(2) 347°
(3)16°
n=563

FIGURE 4

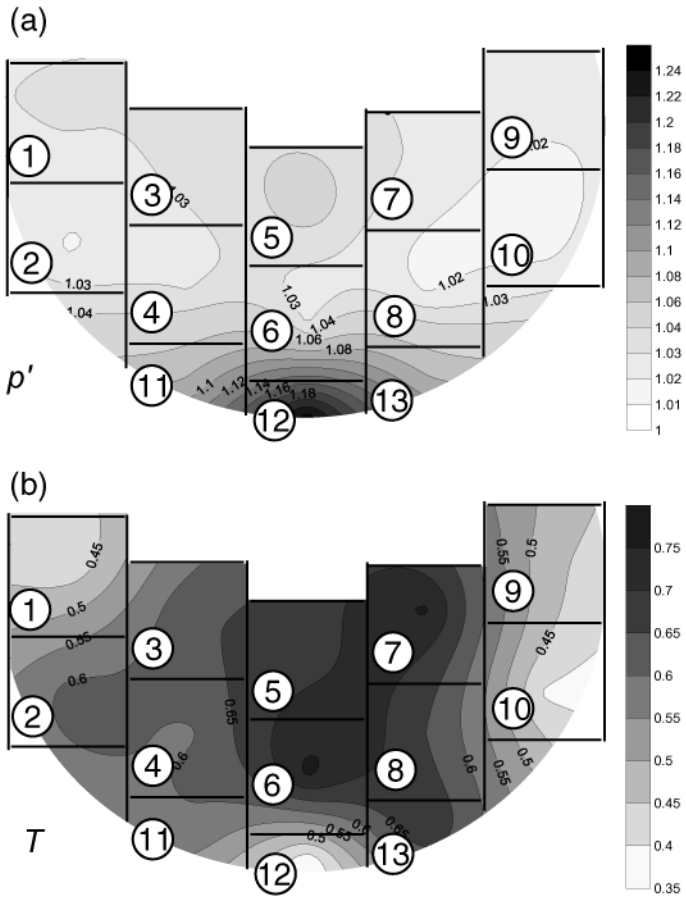
(a)
p′
1.24
1.22
1.2
1.18
1.16
1.14
1.12
1.1
1.08
1.06
1.04
1.03
1.02
1.01
1
(b)
T
0.75
0.7
0.65
0.6
0.55
0.5
0.45
0.4
0.35

FIGURE 5

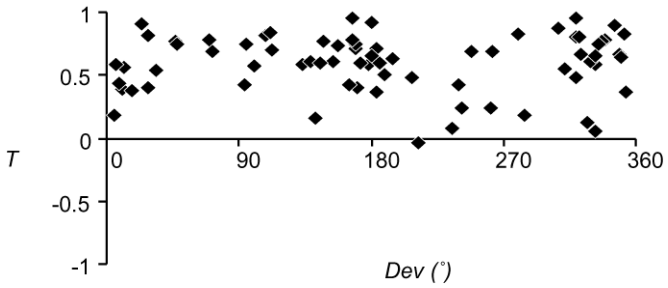

FIGURE 6

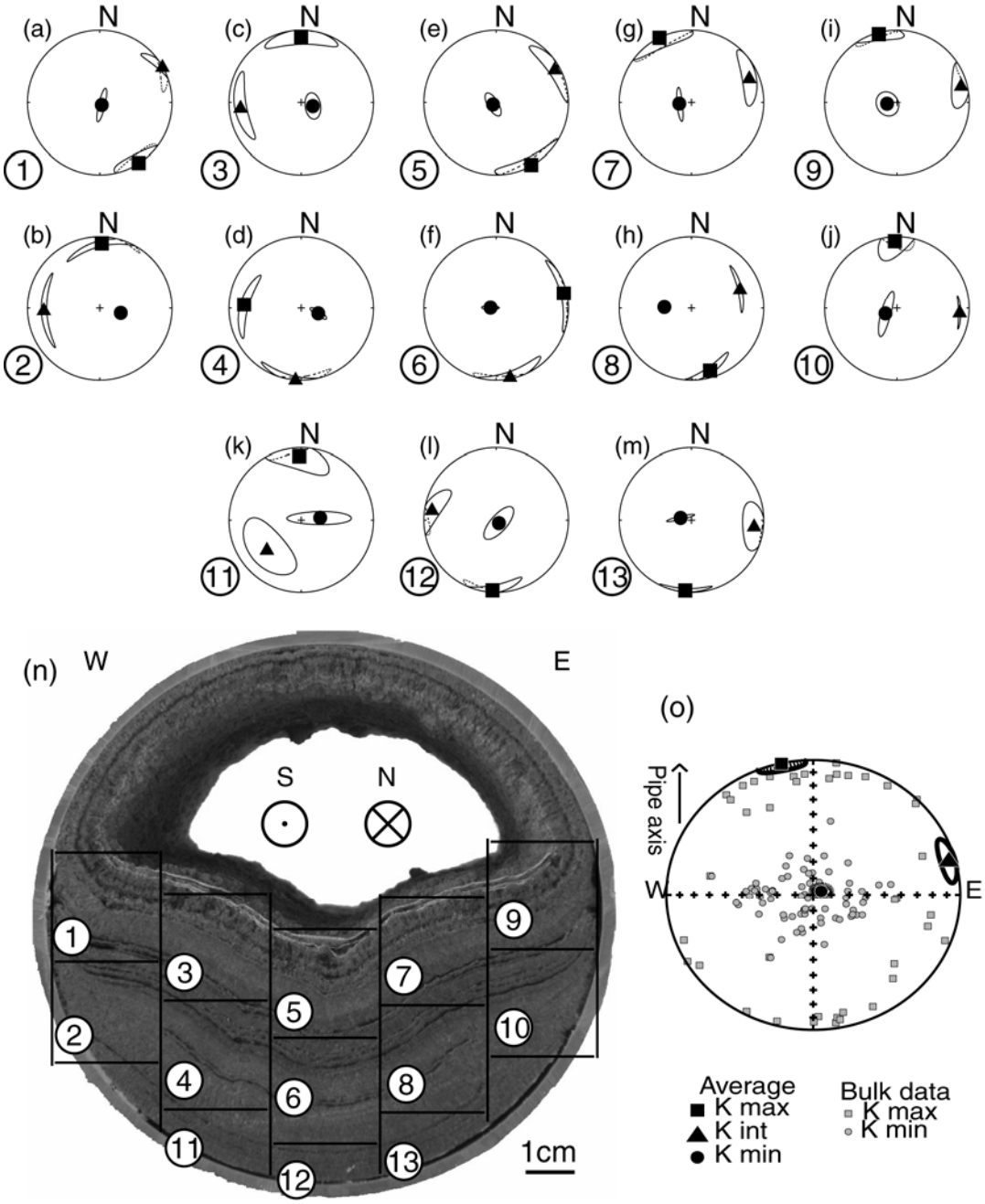
(a)
N
1
(c)
N
3
(e)
N
5
(g)
N
7
(i)
N
9
(b)
N
2
(d)
N
4
(f)
N
6
(h)
N
8
(j)
N
10
(k)
N
11
(l)
N
12
(m)
N
13
(n)
W
E
S
N
1
2
3
4
5
6
7
8
9
10
11
12
13
1cm
(o)
Pipe axis
W
E
Average
K max
K int
K min
Bulk data
K max
K min

FIGURE 7

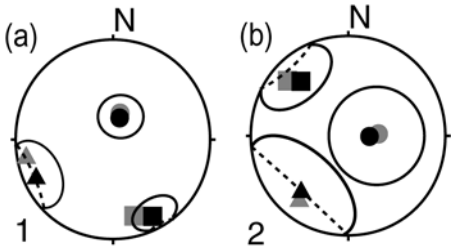

FIGURE 8

Table 1.

Sites	Mrs/Ms	Hcr/Hc
1	0.156	2.48
2	0.194	2.37
3	0.163	2.75
4	0.142	2.15
5	0.160	2.82
6	0.141	2.85
7	0.166	2.86
8	0.164	2.47
9	0.176	2.56
10	0.249	2.10
11	0.151	2.31
12	0.156	1.87
Average	0.168	2.46

Table 2.

Sites	*Kv*	± σ	*P'*	± σ	*T*	± σ	$\mathbf{K_{max}}$		$\mathbf{K_{int}}$		$\mathbf{K_{min}}$	
	(10^{-6} SI)						*D*(°)	*I*(°)	*D*(°)	*I*(°)	*D*(°)	*I*(°)
1	81	28	1...032	0...016	0...41	0...24	147...4	0...9	60...7	0...6	142...4	86...2
2	26	6	1.019	0.005	0.62	0.20	1.9	9.7	267.6	23.8	103.8	65.8
3	82	11	1.034	0.013	0.64	0.15	359.8	10.1	265.5	16.7	107.1	76.2
4	28	5	1.029	0.012	0.59	0.33	273.9	22.4	185.2	0.8	107.5	69.6
5	112	26	1.048	0.005	0.67	0.13	150.7	2.4	60.2	7.7	235.3	85.8
6	24	1	1.031	0.009	0.76	0.13	77.8	3.7	168.7	3.3	273.5	83.5
7	80	12	1.028	0.005	0.76	0.11	333.7	0.7	66.6	13.8	260.1	76.6
8	25	1	1.018	0.002	0.65	0.07	163.6	10.7	67.3	28.4	272.0	58.8
9	44	23	1.021	0.007	0.47	0.19	345.1	2.2	75.4	9.5	260.1	79.1
10	26	10	1.017	0.008	0.39	0.32	358.6	6.6	93.7	14.0	243.1	76.0
11	5	3	1.086	0.036	0.59	0.21	358.5	12.9	229.7	37.8	83.5	68.6
12	10	5	1.256	0.254	0.35	0.58	182.6	4.2	279.2	11	137.3	85.5
13	8	2	1.089	0.020	0.69	0.17	184.5	2.9	95.3	13.9	281.7	77.4
Average	42	10	1.054	0.030	0.585	0.22	348.6	2.2	76.6	3.6	220	87.1